

## High-frequency response analysis via algebraic substructuring

Jin Hwan Ko<sup>1,\*</sup>,<sup>†</sup> and Zhaojun Bai<sup>2,3</sup>

<sup>1</sup>*Department of Aerospace Information Engineering, Konkuk University, Seoul, Korea*

<sup>2</sup>*Department of Computer Science, University of California, Davis, CA 95616, U.S.A.*

<sup>3</sup>*Department of Mathematics, University of California, Davis, CA 95616, U.S.A.*

### SUMMARY

High-frequency response analysis (Hi-FRA) of large-scale dynamical systems is critical to predict the resonant behavior of modern micro-devices and systems operated over MHz or GHz frequency range. Algebraic substructuring (AS) is a powerful technique to extract a large number of natural frequencies. In this work, we extend the AS technique for FRA between two specified cutoff frequencies  $\omega_{\min}$  and  $\omega_{\max}$ . The technique is referred to as ASFRA. ASFRA can be efficiently applied to Hi-FRA, as demonstrated by two examples of microelectromechanical sensors operated at 1–2 and 200–250 MHz ranges. To some extent ASFRA generalizes the underlying numerical algorithm and functionality of commercially viable automated multi-level substructuring (AMLS) technique. AMLS is designed for FRA up to a specific frequency  $\omega_{\max}$ , starting from the lowest, and is inefficient for Hi-FRA. Copyright © 2008 John Wiley & Sons, Ltd.

Received 12 May 2007; Revised 6 January 2008; Accepted 16 January 2008

KEY WORDS: high-frequency response analysis; algebraic substructuring; frequency sweep algorithm; micro-devices

### 1. INTRODUCTION

An engineering structure has many natural frequencies. If it is excited at a frequency close to a natural frequency, resonance occurs. Frequency response analysis (FRA) studies structural responses to steady-state oscillatory excitation to predict the resonant behavior in an operation (excitation) range of frequencies. In the design of macroscale structures, such as an automobile body, one of the main goals is to ensure that natural and excited frequencies are not close to each other to escape undesired resonant vibrations. These frequencies are usually located in a

\*Correspondence to: Jin Hwan Ko, Department of Aerospace Information Engineering, Konkuk University, Seoul, Korea.

<sup>†</sup>E-mail: jhko@aero.konkuk.ac.kr, jinhwanko@gmail.com

Contract/grant sponsor: Korea Research Foundation; contract/grant number: KRF-2005-214-D00015

Contract/grant sponsor: NSF; contract/grant number: DMS-0611548

low-frequency range. However, resonant sensors in microelectromechanical systems and other microscale structures are designed to catch the resonant behavior over a high-frequency range. Therefore, the high FRA (Hi-FRA) is required for the microscale structures. Since they are partially mechanical, most mechanical models are naturally second order in time. The governing equation can be expressed as a continuous time-invariant single-input single-output second-order system:

$$\begin{aligned} M\ddot{x}(t) + D\dot{x}(t) + Kx(t) &= bu(t) \\ y(t) &= l^T x(t) \end{aligned} \quad (1)$$

with the initial conditions  $x(0) = x_0$  and  $\dot{x}(0) = v_0$ . Here  $t$  is the time variable,  $x(t) \in \mathcal{R}^N$  is a state vector,  $N$  is the number of the degree of freedoms.  $u(t)$  is the input excitation force and  $y(t)$  is the output measurement function.  $b \in \mathcal{R}^N$  and  $l \in \mathcal{R}^N$  are the input and output distribution vectors, respectively.  $M, K, D \in \mathcal{R}^{N \times N}$  are system mass, stiffness and damping matrices. It is assumed that  $M$  and  $K$  are symmetric positive definite.  $D$  is a Rayleigh proportional damping, namely  $D = \alpha M + \beta K$  for some scalars  $\alpha$  and  $\beta$ . The input–output behavior of model (1) is characterized by the transfer function:

$$H(\omega) = l^T (K + i\omega D - \omega^2 M)^{-1} b \quad (2)$$

where  $\omega$  is the frequency and  $i = \sqrt{-1}$ .

Mathematically speaking, the FRA is on the computation of the transfer function  $H(\omega_k)$  for a set of frequencies  $\omega_k$  in a specific frequency interval  $[\omega_{\min}, \omega_{\max}]$ . For large-scale systems (1), it is prohibitive to directly compute  $H(\omega_k)$  for a large number of frequency points  $\omega_k \in [\omega_{\min}, \omega_{\max}]$ . A popular approach is to apply an eigensystem analysis, known as the mode superposition (MS) method, see [1], for example. One first extracts  $n$  eigenpairs  $(\lambda_k, q_k)$  of the matrix pair  $(K, M)$ :

$$Kq_k = \lambda_k Mq_k \quad (3)$$

where the eigenvector  $q_k$  is normalized, i.e.  $q_k^T M q_k = 1$ . Then by projecting the transfer function  $H(\omega)$  onto the subspace  $\text{span}\{Q_n\} = \text{span}\{[q_1, q_2, \dots, q_n]\}$ , it yields an approximation of  $H(\omega)$ :

$$H_n(\omega) = l_n^T (\Lambda_n + i\omega D_n - \omega^2 I_n)^{-1} b_n \quad (4)$$

where  $\Lambda_n = \text{diag}(\lambda_1, \lambda_2, \dots, \lambda_n)$ ,  $D_n = Q_n^T D Q_n$ ,  $l_n = Q_n^T l$  and  $b_n = Q_n^T b$ . In practice, it is often that  $H_n(\omega)$  reaches to sufficient accuracy for an  $n$  which is much smaller than  $N$ . The selection of the eigenpairs  $(\lambda_k, q_k)$  depends on the frequency range of interest. The shift-and-invert Lanczos (SIL) method as an eigensolver has been the method of choice for decades, see [2] and references therein.

However, the continual and compelling needs for FRA of very large system (1) challenge the computational efficiency of SIL method. Substructuring approaches, initially developed in early 1960s, have revitalized in recent years. The automated multi-level substructuring (AMLS) method is one of the modern substructuring approaches and has already become a commercial viable application [3–6]. The substructuring approaches partition initial structures, namely coefficient matrices of system (1), into a number of substructures, each of which is composed of substructures, and so on. These substructures can be handled efficiently on single or multiprocessor computing environment. A variation of the AMLS technique, referred to as the algebraic substructuring (AS) method, is studied in [7–9]. In this work, we extend the AS method for FRA between two specified cutoff frequencies  $\omega_{\min}$  and  $\omega_{\max}$ . The technique is referred to as ASFRA. To some extent ASFRA

generalizes the underlying numerical algorithm and functionality of the AMLS technique, which is designed for FRA up to a specified cutoff frequency  $\omega_{\max}$ , starting from the lowest. Therefore, AMLS is computationally inefficient for Hi-FRA.

The rest of this paper is organized as follows. In Section 2, we review the AS method for extracting modal subspace. In Section 3, we present a generalization of the frequency sweep (FS) strategy first proposed in [4, 6]. Section 4 presents a summary of the FRA using AS method. The FRA of two microelectromechanical sensors operated at 1–2 and 200–250 MHz ranges is presented in Section 5. Concluding remarks are in Section 6.

## 2. ALGEBRAIC SUBSTRUCTURING

For Hi-FRA the eigenmodes corresponding to the natural frequency in the operation range are most important. Hence we start from an eigensystem of a shifted pair  $(K^\sigma, M)$ :

$$K^\sigma q = \lambda^\sigma M q \tag{5}$$

where  $K^\sigma = K - \sigma M$  and  $\lambda^\sigma = \lambda - \sigma$ . We assume that the rows and columns of  $K^\sigma$  and  $M$  have been permuted and partitioned of the forms:

$$K^\sigma = \begin{matrix} & \begin{matrix} N_1 & N_2 & N_3 \end{matrix} \\ \begin{matrix} N_1 \\ N_2 \\ N_3 \end{matrix} & \begin{bmatrix} K_{11}^\sigma & & K_{13}^\sigma \\ & K_{22}^\sigma & K_{23}^\sigma \\ K_{31}^\sigma & K_{32}^\sigma & K_{33}^\sigma \end{bmatrix} \end{matrix} \quad \text{and} \quad M = \begin{matrix} & \begin{matrix} N_1 & N_2 & N_3 \end{matrix} \\ \begin{matrix} N_1 \\ N_2 \\ N_3 \end{matrix} & \begin{bmatrix} M_{11} & & M_{13} \\ & M_{22} & M_{23} \\ M_{31} & M_{32} & M_{33} \end{bmatrix} \end{matrix} \tag{6}$$

where  $N_1, N_2$  and  $N_3$  indicate the orders of sub-matrix blocks. The pairs  $(K_{11}^\sigma, M_{11})$  and  $(K_{22}^\sigma, M_{22})$  define substructure blocks that are connected by the interface pairs  $(K_{33}^\sigma, M_{33})$ . In a pure algebraic setting, permutation and partition can be accomplished by applying a matrix ordering and partitioning algorithm such as a nested dissection algorithm to the algebraic structure of  $|K^\sigma| + |M|$ , see [10].

For the simplicity of exposition we only show a single-level AS method. Multi-level AS method has been implemented and used for numerical experiments in Section 5. The AS method begins with a block LDL<sup>T</sup> factorization of  $K^\sigma$ :

$$K^\sigma = L^T \widehat{K}^\sigma L \tag{7}$$

where

$$\widehat{K}^\sigma = \begin{bmatrix} K_{11}^\sigma & & \\ & K_{22}^\sigma & \\ & & \widehat{K}_{33}^\sigma \end{bmatrix} \quad \text{and} \quad L = \begin{bmatrix} I & (K_{11}^\sigma)^{-1} K_{13}^\sigma \\ & I & (K_{22}^\sigma)^{-1} K_{23}^\sigma \\ & & I \end{bmatrix}$$

and  $\widehat{K}_{33}^\sigma = K_{33}^\sigma - \sum_{i=1}^2 (K_{i3}^\sigma)^T (K_{ii}^\sigma)^{-1} K_{i3}^\sigma$ . By performing a congruent transformation of the matrix pair  $(\widehat{K}^\sigma, M)$  using matrix  $L$ , the shifted eigenvalue problem (5) is transformed into the eigenvalue problem:

$$\widehat{K}^\sigma \widehat{q} = \lambda^\sigma \widehat{M} \widehat{q} \tag{8}$$

where  $\hat{q} = Lq$ ,  $\hat{K}^\sigma = L^{-T} K^\sigma L^{-1}$  as defined in (7),

$$\hat{M} = L^{-T} M L^{-1} = \begin{bmatrix} M_{11} & & \hat{M}_{13} \\ & M_{22} & \hat{M}_{23} \\ \hat{M}_{31} & \hat{M}_{32} & \hat{M}_{33} \end{bmatrix}$$

and

$$\hat{M}_{i3} = M_{i3} - M_{ii}(K_{ii}^\sigma)^{-1} K_{i3}^\sigma$$

$$\hat{M}_{33} = M_{33} - \sum_{i=1}^2 \{ (K_{i3}^\sigma)^T (K_{ii}^\sigma)^{-1} M_{i3} + M_{i3}^T (K_{ii}^\sigma)^{-1} K_{i3}^\sigma - (K_{i3}^\sigma)^T (K_{ii}^\sigma)^{-1} M_{ii} (K_{ii}^\sigma)^{-1} K_{i3}^\sigma \}$$

The structure of the matrix pair  $(\hat{K}^\sigma, \hat{M})$  is known as the Craig–Bampton form in structural engineering [11].

The next step of the AS is to extract the eigenpairs of interior submatrix pairs  $(K_{ii}^\sigma, M_{ii})$  for  $i = 1, 2$  and the interface pair  $(\hat{K}_{33}^\sigma, \hat{M}_{33})$ . These eigenvectors are referred to as *local modes*. The local modes to be extracted are those eigenvectors whose corresponding eigenvalues are between *local cutoff values*  $\mu_{\min}^\sigma$  and  $\mu_{\max}^\sigma$ . In Section 4 we will discuss how to decide these local cutoff values with respect to the prescribed frequency range  $[\omega_{\min}, \omega_{\max}]$  of interest.

Let us define

$$S_m = \begin{matrix} & m_1 & m_2 & m_3 \\ \begin{matrix} N_1 \\ N_2 \\ N_3 \end{matrix} & \begin{bmatrix} S_1 & & \\ & S_2 & \\ & & S_3 \end{bmatrix} \end{matrix}$$

where  $S_1$ ,  $S_2$  and  $S_3$  consist of  $m_1$ ,  $m_2$  and  $m_3$  extracted local modes of the submatrix pairs  $(K_{11}^\sigma, M_{11})$ ,  $(K_{22}^\sigma, M_{22})$  and  $(\hat{K}_{33}^\sigma, \hat{M}_{33})$ , respectively.  $m = m_1 + m_2 + m_3$ .

Projecting the matrix pair  $(\hat{K}^\sigma, \hat{M})$  onto the subspace  $\text{span}\{S_m\}$  yields a reduced eigensystem:

$$K_m^\sigma \phi = \theta^\sigma M_m \phi \quad (9)$$

where  $K_m^\sigma$  and  $M_m$  are  $m \times m$  matrices defined as

$$K_m^\sigma = S_m^T \hat{K}^\sigma S_m \quad \text{and} \quad M_m = S_m^T \hat{M} S_m \quad (10)$$

Note that by the definition of the local modes, matrix  $K_m^\sigma$  is diagonal. The diagonal elements of  $K_m^\sigma$  are the extracted eigenvalues of the interior submatrix pairs  $(K_{ii}^\sigma, M_{ii})$  and the interface submatrix pair  $(\hat{K}_{33}^\sigma, \hat{M}_{33})$ . We will call  $(K_m^\sigma, M_m)$  as an *AS matrix pair*. The eigenvectors  $\{\phi\}$  of the AS matrix pair  $(K_m^\sigma, M_m)$  will be referred to as *global modes*. The subspace spanned by the columns of the matrix  $L^{-1} S_m$  is called an *AS subspace*.

To end this section, we note that for eigenvalue computation by the AS method, the eigenpairs  $(\lambda, q)$  of the original matrix pair  $(K, M)$  are approximated by the Ritz pairs:

$$(\theta^\sigma + \sigma, L^{-1} S_m \phi)$$

For discussion on the quality of these approximate eigenpairs, see [7, 9] and reference therein.

## 3. FREQUENCY RESPONSE ANALYSIS

In this section, we discuss the FRA after extracting the AS subspace as described in the previous section. First, for the Rayleigh damping  $D = \alpha M + \beta K$ , the original frequency response  $H(\omega)$  defined in (2) can be rewritten as

$$H(\omega) = l^T (\gamma_1 K^\sigma + \gamma_2 M)^{-1} b = l^T p(\omega)$$

where

$$\gamma_1 = \gamma_1(\omega) = 1 + i\omega\beta \quad \text{and} \quad \gamma_2 = \gamma_2(\omega, \sigma) = -\omega^2 + \sigma + i\omega(\alpha + \sigma\beta)$$

and  $p(\omega)$  is the solution of parameterized linear system

$$G(\omega)p(\omega) = (\gamma_1 K^\sigma + \gamma_2 M)p(\omega) = b$$

It is also referred to as the frequency response equation in structural engineering.

By projecting the frequency response equation onto the AS subspace  $\text{span}\{L^{-1}S_m\}$ , we have an approximate frequency response  $H_m(\omega)$  of  $H(\omega)$ :

$$H_m(\omega) = l_m^T (\gamma_1 K_m^\sigma + \gamma_2 M_m)^{-1} b_m = l_m^T p_m(\omega) \quad (11)$$

where  $K_m^\sigma$  and  $M_m$  are defined as (10), and  $l_m = (L^{-1}S_m)^T l$  and  $b_m = (L^{-1}S_m)^T b$ . The vector  $p_m(\omega)$  is the solution of the projected frequency response equation

$$G_m(\omega)p_m(\omega) = (\gamma_1 K_m^\sigma + \gamma_2 M_m)p_m(\omega) = b_m \quad (12)$$

Owing to the fact that a large number of local modes are typically needed to have an accurate representation of the global modes, the order  $m$  of the projected equation (12) is still too high to directly calculate the responses  $p_m(\omega_k)$  for a large number of frequencies  $\omega_k$ . A so-called FS scheme is introduced in the AMLS method [4, 6]. The FS scheme is based on the observation that the response  $p_m(\omega)$  with respect to most global modes changes slowly with frequency, except to those modes that are close to resonance. Therefore, we can separate the response into two components, one associated with nearly resonant global modes, they are typically few in number, and the second one for the response that varies slowly with frequency. For the purpose of efficient Hi-FRA as described in this paper, it is also important to be able to identify those global modes corresponding to the frequency range  $[\omega_{\min}, \omega_{\max}]$  of interest. In the following, we provide a rigorous mathematical derivation of the FS scheme for the Hi-FRA application. The derivation uses a different approach from the one to derive the FS scheme in AMLS [4, 6].

For Hi-FRA, we partition the global modes  $\Phi = (\phi)$  into three groups according to the location of their corresponding eigenvalues  $\Theta^\sigma = (\theta^\sigma)$ :

- (1)  $\Phi_n$  are the retained global modes, whose corresponding eigenvalues  $\Theta_n^\sigma$  are in an interval  $[\lambda_{\min}^\sigma, \lambda_{\max}^\sigma]$  determined by the excitation frequency range  $[\omega_{\min}, \omega_{\max}]$ .  $\lambda_{\min}^\sigma$  and  $\lambda_{\max}^\sigma$  are referred to as (*left and right*) *global cutoff values*.
- (2)  $\Phi_l$  are the global modes whose corresponding eigenvalues  $\Theta_l^\sigma$  are smaller than the left global cutoff value  $\lambda_{\min}^\sigma$ .
- (3)  $\Phi_r$  are those global modes whose corresponding eigenvalues  $\Theta_r^\sigma$  are larger than the right global cutoff value  $\lambda_{\max}^\sigma$ .

The *truncated modes*, which are not computed in practice, are referred to the global modes  $\Phi_l$  and  $\Phi_r$ . By writing

$$\Phi = [\Phi_l \ \Phi_n \ \Phi_r] \quad (13)$$

an eigendecomposition of the matrix pair  $(K_m^\sigma, M_m)$  is given by

$$\Phi^T K_m^\sigma \Phi = \Theta^\sigma = \text{diag}(\Theta_l^\sigma, \Theta_n^\sigma, \Theta_r^\sigma) \quad \text{and} \quad \Phi^T M_m \Phi = I \quad (14)$$

With the partition of the global modes, the response  $p_m(\omega)$  of the frequency response equation (12) be decomposed into two parts as

$$p_m(\omega) = p_n(\omega) + p_t(\omega) \quad (15)$$

where  $p_n(\omega)$  is in the subspace spanned by the retained global modes  $\Phi_n$  and represents the response for modes whose natural frequency is to be retained.  $p_t(\omega)$  is in the subspace spanned by the truncated modes  $\Phi_l$  and  $\Phi_r$  and represents the response for modes whose natural frequency are truncated. It is easy to verify that  $p_n(\omega)$  and  $p_t(\omega)$  satisfy the orthogonality conditions:

$$p_n^T(\omega) K_m^\sigma p_t(\omega) = 0 \quad \text{and} \quad p_n^T(\omega) M_m p_t(\omega) = 0 \quad (16)$$

Writing  $p_n(\omega) = \Phi_n \eta_n(\omega)$  for some coefficient vector  $\eta_n(\omega)$ , the projected frequency response equation (12) becomes

$$G_m(\omega) [\Phi_n \eta_n(\omega) + p_t(\omega)] = b_m \quad (17)$$

Pre-multiplying the equation by  $\Phi_n^T$  and applying the orthogonality condition (16), the  $p_n(\omega)$ -component of the response  $p_m(\omega)$  is immediately given by

$$\begin{aligned} p_n(\omega) &= \Phi_n \eta_n(\omega) \\ &= \Phi_n [\Phi_n^T G_m(\omega) \Phi_n]^{-1} \Phi_n^T b_m \\ &= \Phi_n (\gamma_1 \Theta_n^\sigma + \gamma_2 I)^{-1} \Phi_n^T b_m \end{aligned} \quad (18)$$

After  $p_n(\omega)$  is computed, the frequency response equation (17) can be rewritten as a parameterized linear system for the  $p_t(\omega)$ -component of the response  $p_m(\omega)$ :

$$G_m(\omega) p_t(\omega) = e_n(\omega) \quad (19)$$

where  $e_n(\omega)$  is a partial residual vector corresponding to the frequency response solution component  $p_n(\omega)$ :

$$e_n(\omega) = b_m - G_m(\omega) p_n(\omega)$$

Since it is anticipated that truncated response  $p_t(\omega)$  varies slowly with frequency, we use an iterative refinement scheme for an inexpensive update of  $p_t(\omega)$  as frequency changes, with the most recent approximation as an initial guess. Specifically, we express

$$p_t^\ell(\omega) = p_t^{\ell-1}(\omega) + \Delta p_t^\ell(\omega) \quad (20)$$

where the correction term  $\Delta p_t^\ell(\omega)$  is the solution of the refinement equation

$$G_m(\omega) \Delta p_t^\ell(\omega) = r_m^{\ell-1}(\omega) \quad (21)$$

where  $r_m^{\ell-1}(\omega)$  is the residual of the  $(\ell-1)$ th approximation solution  $p_m^{\ell-1}(\omega) = p_n(\omega) + p_t^{\ell-1}(\omega)$  of the frequency response equation (12), defined as

$$\begin{aligned} r_m^{\ell-1}(\omega) &= b_m - G_m(\omega)p_m^{\ell-1}(\omega) \\ &= b_m - G_m(\omega)[p_n(\omega) + p_t^{\ell-1}(\omega)] \\ &= e_n(\omega) - G_m(\omega)p_t^{\ell-1}(\omega) \end{aligned} \quad (22)$$

To solve the refinement equation (21) by the Galerkin subspace projection technique, see [12], for example, we seek  $\Delta p_t^\ell(\omega)$  such that

$$\Delta p_t^\ell(\omega) \in \text{span}\{\Phi_t\} \quad \text{and} \quad G_m(\omega)\Delta p_t^\ell(\omega) - r_m^{\ell-1}(\omega) \perp \text{span}\{\Phi_t\} \quad (23)$$

where  $\Phi_t$  are all truncated modes,  $\Phi_t = [\Phi_l \ \Phi_r]$ . Condition (23) is equivalent to find a vector  $\Delta \eta_t^\ell(\omega)$  such that

$$\Delta p_t^\ell(\omega) = \Phi_t \Delta \eta_t^\ell(\omega) \quad \text{and} \quad \Phi_t^T [G_m(\omega)\Phi_t \Delta \eta_t^\ell(\omega) - r_m^{\ell-1}(\omega)] = 0 \quad (24)$$

Hence we have

$$\Delta \eta_t^\ell(\omega) = [\Phi_t^T G_m(\omega)\Phi_t]^{-1} \Phi_t^T r_m^{\ell-1}(\omega)$$

and

$$\begin{aligned} \Delta p_t^\ell(\omega) &= \Phi_t (\Phi_t^T G_m(\omega)\Phi_t)^{-1} \Phi_t^T r_m^{\ell-1}(\omega) \\ &= \Phi_t (\gamma_1 \Theta_t^\sigma + \gamma_2 I)^{-1} \Phi_t^T r_m^{\ell-1}(\omega) \end{aligned} \quad (25)$$

Since the truncation modes  $\Phi_t$  are not explicitly computed in practice, by some algebraic manipulation, the right-hand side of Equation (25) can be reformulated in terms of the matrix pair  $(K_m^\sigma, M_m)$  and the retained modes  $\Phi_n$  as follows:

$$\Delta p_t^\ell(\omega) = [(\gamma_1 K_m^\sigma + \gamma_2 M_m)^{-1} - \Phi_n (\gamma_1 \Theta_n^\sigma + \gamma_2 I)^{-1} \Phi_n^T] r_m^{\ell-1}(\omega) \quad (26)$$

To reduce the computational expenses, one may ignore the term  $\gamma_2 I$  in the correction term of the truncated response (25) and lead to an inexpensive stationary iteration that converges. This is equivalent to ignoring the terms  $\gamma_2 M_m$  and  $\gamma_2 I$  in (26):

$$\Delta p_t^\ell(\omega) \approx \Phi_t (\gamma_1 \Theta_t^\sigma)^{-1} \Phi_t^T r_m^{\ell-1}(\omega) \quad (27)$$

$$= \frac{1}{\gamma_1} [(K_m^\sigma)^{-1} - \Phi_n (\Theta_n^\sigma)^{-1} \Phi_n^T] r_m^{\ell-1}(\omega) \quad (28)$$

Recall that  $K_m^\sigma$  is diagonal. Subsequently, we derive the following so-called *FS iteration* for computing the truncated response  $p_t(\omega)$ :

$$p_t^\ell(\omega) = p_t^{\ell-1}(\omega) + \frac{1}{\gamma_1} [(K_m^\sigma)^{-1} - \Phi_n (\Theta_n^\sigma)^{-1} \Phi_n^T] r_m^{\ell-1}(\omega) \quad (29)$$

for  $\ell = 1, 2, \dots$ , with the given initial  $p_t^0(\omega)$ .

A natural choice of the initial approximation  $p_t^0(\omega)$  is to use a linear extrapolation from the truncated responses  $p_t(\omega)$  at the most recent frequency points. Specifically, assume that we wish to calculate the  $n_f$  frequency points  $\omega_k$  for  $i = 1, 2, \dots, n_f$ , such that

$$\omega_{\min} \leq \omega_1 < \omega_2 < \dots < \omega_{n_f} \leq \omega_{\max}$$

We can use two recent approximations  $p_t(\omega_{k-1})$  and  $p_t(\omega_{k-2})$  at the frequency points  $\omega_{k-1}$  and  $\omega_{k-2}$  to obtain an initial response  $p_t^0(\omega_k)$  for the frequency point  $\omega_k$ , via a simple linear extrapolation:

$$p_t^0(\omega_k) = p_t(\omega_{k-1}) + \frac{\omega_k - \omega_{k-1}}{\omega_{k-1} - \omega_{k-2}} (p_t(\omega_{k-1}) - p_t(\omega_{k-2})) \quad (30)$$

for  $k = 3, 4, \dots, n_f$ , where initially we simply set  $p_t^0(\omega_1) = 0$  and  $p_t^0(\omega_2) = p_t(\omega_1)$ .

By Equation (27) and the choice of initial response in (30), it is easy to see that  $p_t^\ell(\omega_k)$  generated by the FS iteration (29) is in the subspace spanned by the truncated modes  $\Phi_t$ ,

$$p_t^\ell(\omega_k) \in \text{span}\{\Phi_t\}$$

Therefore,  $p_t^\ell(\omega_k)$  satisfies to the orthogonality condition (16), i.e.

$$p_n^T(\omega_k) K_m^\sigma p_t^\ell(\omega_k) = 0 \quad \text{and} \quad p_n^T(\omega_k) M_m p_t^\ell(\omega_k) = 0$$

A practical stopping criterion for the FS iteration (29) is by the relative residual error

$$\frac{\|\Delta p_t^\ell(\omega)\|_2}{\|(\gamma_1 K_m^\sigma)^{-1} b_m\|_2} \leq \varepsilon \quad (31)$$

where  $\varepsilon$  is a prescribed tolerance value.

Combining expression (18) for the component  $p_n(\omega)$  and the FS iteration (29) for the component  $p_t^\ell(\omega)$ , we essentially have an algorithm for computing the solution  $p_m(\omega)$  of the frequency response equation (12). A key remaining question is what are those global modes  $\Phi_n$  to be retained and computed explicitly. In other words, we need to derive a relationship between the prescribed frequency range  $[\omega_{\min}, \omega_{\max}]$  of interest and the global cutoff values  $\lambda_{\min}^\sigma$  and  $\lambda_{\max}^\sigma$  for those global modes  $\Phi_n$  to be retained explicitly. Our approach to address this question is to extend the elegant idea described in [4, 6] by searching for a condition to guarantee the convergence of the FS iteration (29).

Taking the norm on both sides of expression (27), we have

$$\begin{aligned} \|\Delta p_t^\ell(\omega)\|_2 &\approx \|\Phi_t (\gamma_1 \Theta_t^\sigma)^{-1} \Phi_t^T r_m^{\ell-1}(\omega)\|_2 \\ &\leq \|\Phi_t (\gamma_1 \Theta_t^\sigma)^{-1}\|_2 \|\Phi_t^T r_m^{\ell-1}(\omega)\|_2 \end{aligned} \quad (32)$$

The term  $\Phi_t^T r_m^{\ell-1}(\omega)$  is called a *truncated modal residual*. For the convergence of the FS iteration (29), we wish to decrease  $\|\Delta p_t^\ell(\omega)\|_2$ , which implies to keep the norm of truncated modal residual decreasing. To this end, we exploit the relationship between two consecutive truncated modal residuals. First, we note that two consecutive residuals  $r_m^{\ell-1}(\omega)$  and  $r_m^\ell(\omega)$  corresponding to the

$(\ell - 1)$ th and  $\ell$ th iterates  $p_m^{\ell-1}(\omega)$  and  $p_m^\ell(\omega)$  are related as follows:

$$\begin{aligned}
 r_m^\ell(\omega) &= b_m - G_m(\omega)p_m^\ell(\omega) \\
 &= b_m - G_m(\omega)(\Phi_n \eta_n(\omega) + p_t^\ell(\omega)) \\
 &= r_m^{\ell-1}(\omega) - \frac{1}{\gamma_1} G_m(\omega)((K_m^\sigma)^{-1} - \Phi_n(\Theta_n^\sigma)^{-1}\Phi_n^T)r_m^{\ell-1}(\omega) \\
 &= \left[ I - \frac{1}{\gamma_1} G_m(\omega)((K_m^\sigma)^{-1} - \Phi_n(\Theta_n^\sigma)^{-1}\Phi_n^T) \right] r_m^{\ell-1}(\omega) \\
 &= \left[ I - \frac{1}{\gamma_1} (\gamma_1 K_m^\sigma + \gamma_2 M_m)((K_m^\sigma)^{-1} - \Phi_n(\Theta_n^\sigma)^{-1}\Phi_n^T) \right] r_m^{\ell-1}(\omega) \\
 &= \left[ K_m^\sigma \Phi_n(\Theta_n^\sigma)^{-1}\Phi_n^T - \frac{\gamma_2}{\gamma_1} M_m((K_m^\sigma)^{-1} - \Phi_n(\Theta_n^\sigma)^{-1}\Phi_n^T) \right] r_m^{\ell-1}(\omega) \tag{33}
 \end{aligned}$$

Pre-multiplying (33) with  $\Phi_t^T$  and using the orthogonality condition (16) yields

$$\Phi_t^T r_m^\ell(\omega) = -\frac{\gamma_2}{\gamma_1} \Phi_t^T M_m (K_m^\sigma)^{-1} r_m^{\ell-1}(\omega) \tag{34}$$

By the definition of  $\Phi$  in Equation (13) and the eigendecomposition (14), we have the following expression for two consecutive truncated modal residuals:

$$\begin{aligned}
 \Phi_t^T r_m^\ell(\omega) &= -\frac{\gamma_2}{\gamma_1} \Phi_t^T M_m \Phi(\Theta^\sigma)^{-1} \Phi^T r_m^{\ell-1}(\omega) \\
 &= -\frac{\gamma_2}{\gamma_1} \begin{bmatrix} I_l & 0 & 0 \\ 0 & 0 & I_r \end{bmatrix} (\Theta^\sigma)^{-1} \Phi^T r_m^{\ell-1}(\omega) \\
 &= -\frac{\gamma_2}{\gamma_1} \begin{bmatrix} \Theta_l^\sigma & \\ & \Theta_r^\sigma \end{bmatrix}^{-1} \Phi_t^T r_m^{\ell-1}(\omega) \tag{35}
 \end{aligned}$$

In a componentwise form the ratio in the absolute value between two consecutive truncated modal residuals is given by

$$\left| \frac{\phi_k^T r_m^\ell(\omega)}{\phi_k^T r_m^{\ell-1}(\omega)} \right| = \frac{d(\omega, \sigma)}{|\theta_k^\sigma|} \tag{36}$$

where  $\phi_k$  is one of the truncated modes  $\Phi_t$ , and  $d(\omega, \sigma)$  is given by

$$d(\omega, \sigma) = \left| -\frac{\gamma_2}{\gamma_1} \right| = \frac{\sqrt{(\omega^2 - \sigma)^2 + \omega^2(\alpha + \beta\sigma)^2}}{\sqrt{1 + \omega^2\beta^2}}$$

Let  $d_{\max} = \max\{d(\omega_k, \sigma), 1 \leq k \leq n_f\}$ . Then if we introduce a positive constant  $\xi$ , referred to as *contraction ratio*, such that

$$\left| \frac{\phi_k^T r_m^\ell(\omega)}{\phi_k^T r_m^{\ell-1}(\omega)} \right| \leq \frac{d_{\max}}{|\theta_k^\sigma|} \leq \xi < 1 \tag{37}$$

then the components of the truncated modal residual  $\Phi_t^T r_m^\ell(\omega)$  are enforced to be contracted, namely

$$|\phi_k^T r_m^\ell(\omega)| \leq \xi |\phi_k^T r_m^{\ell-1}(\omega)| \leq \xi^\ell |\phi_k^T r_m^0(\omega)| \rightarrow 0 \quad \text{as } \ell \rightarrow \infty$$

Subsequently, the norm of the correction term  $\Delta p_t(\omega)$  in (32) decreases and the FS iteration (29) converges. Moreover, by the contraction condition (37), it suggests that the global modes corresponding to the eigenvalues  $\theta^\sigma$  of the matrix pair  $(K_m^\sigma, M_m)$  outside the interval  $[-d_{\max}/\xi, d_{\max}/\xi]$  can be cut off. Hence, the global cutoff values  $\lambda_{\min}^\sigma$  and  $\lambda_{\max}^\sigma$ , with respect to the shifted matrix pair  $(K^\sigma, M)$ , are defined as

$$\lambda_{\min}^\sigma = -\frac{d_{\max}}{\xi} \quad \text{and} \quad \lambda_{\max}^\sigma = \frac{d_{\max}}{\xi} \tag{38}$$

In other words, the eigenpairs of the original matrix pair  $(K, M)$  corresponding to the interval

$$[\lambda_{\min}, \lambda_{\max}] = [\lambda_{\min}^\sigma + \sigma, \lambda_{\max}^\sigma + \sigma] = \left[ \sigma - \frac{d_{\max}}{\xi}, \sigma + \frac{d_{\max}}{\xi} \right]$$

should be computed explicitly and retained.

When there is no shift, i.e.  $\sigma = 0$ , the left global cutoff value  $\lambda_{\min}^0$  is set to be zero. The retained global modes are those eigenvectors of  $(K_m^0, M_m)$  whose corresponding eigenvalues are smaller than

$$\lambda_{\max}^0 = \frac{1}{\xi} d(\omega_{\max}, 0) = \frac{\omega_{\max}}{\xi} \sqrt{\frac{\omega_{\max}^2 + \alpha^2}{1 + \omega_{\max}^2 \beta^2}} \tag{39}$$

i.e. the eigenpairs of the original matrix pair  $(K, M)$  corresponding to the interval

$$[0, \lambda_{\max}] = [0, \lambda_{\max}^0] = \left[ 0, \frac{d(\omega_{\max}, 0)}{\xi} \right]$$

should be computed explicitly and retained. This is consistent with the choice of the cutoff value of the AMLS for FRA up to a specified frequency, starting from the lowest [4, 6].

#### 4. ASFRA

By combining the AS method for extracting global modes in Section 2 and the frequency response algorithm in Section 3, we have an algorithm for computing the frequency responses  $H(\omega_k)$  for a set of frequency points  $\omega_k$  over an arbitrary interval  $[\omega_{\min}, \omega_{\max}]$ . The algorithm is referred to as the ASFRA algorithm which stands for algebraic substructuring-based algorithm for FRA.

As we have seen in Sections 2 and 3, ASFRA involves a number of parameters. The performance of ASFRA depends on the choice of these parameters. An in-depth study of optimal parameter

selection is beyond the scope of this paper. In the following, we give a brief discussion on the choice of the parameters and the default values we have used.

- Shift  $\sigma$ : It is necessary that the shift  $\sigma$  is chosen in the interval  $[\omega_{\min}^2, \omega_{\max}^2]$  for better accuracy of the eigenvalues associated with the global modes within the range. The center point of the frequency range is the default value,  $\sigma = \frac{1}{2}(\omega_{\min}^2 + \omega_{\max}^2)$ .
- Substructuring level  $l_v$ : This is an important parameter to affect the accuracy and performance of the AS method. The choice of  $l_v$  is beyond the scope of this paper, see [6, 8, 9] for the discussion. The default value is  $l_v = 3$ .
- Global cutoff values  $\lambda_{\min}^\sigma$  and  $\lambda_{\max}^\sigma$ : By (38),  $\lambda_{\min}^\sigma$  and  $\lambda_{\max}^\sigma$  are essentially determined by the contraction ratio  $\xi$ . To improve the convergence of the FS iteration (29), the contraction ratio  $\xi$  should be small. However, it increases the number of retained global modes. We use  $\xi = 0.5$  as the default value. A preliminary study of the impact of  $\xi$  is reported in Section 5.
- Local cutoff values  $\mu_{\min}^\sigma$  and  $\mu_{\max}^\sigma$ : The impact of local modes on the accuracy of global modes has been an important issue in the study of the AS algorithm [7, 9]. To achieve a desired level of accuracy of the global modes, a large number of local modes are typically required. In the study of FRA, the local cutoff values  $\mu_{\min}^\sigma$  and  $\mu_{\max}^\sigma$  are chosen proportionally to the global cutoff values  $\lambda_{\min}^\sigma$  and  $\lambda_{\max}^\sigma$ , namely

$$\mu_{\min}^\sigma = c_l \lambda_{\min}^\sigma \quad \text{and} \quad \mu_{\max}^\sigma = c_u \lambda_{\max}^\sigma$$

where  $c_l$  and  $c_u$  are relaxation factors. In general, more local modes are retained when  $c_l$  and  $c_u$  are larger. Consequently, the accuracy of the global modes is also improved. The default value is  $c_l = c_u = 10$ . We have a preliminary study of the impact of the choice  $c_l = c_u$  in Section 5 for two numerical experiments.

- The tolerance value  $\varepsilon$  for stopping criterion (31) of the FS iteration (29) is set to  $\varepsilon = 10^{-5}$ , as a default value.

In summary, the following is a pseudocode of the complete ASFRA algorithm for computing frequency responses  $H(\omega_k)$  at  $n_f$  prescribed frequency points  $\{\omega_k, k = 1, 2, \dots, n_f\}$  satisfying  $\omega_{\min} \leq \omega_1 < \omega_2 < \dots < \omega_{n_f} \leq \omega_{\max}$ .

#### ASFRA

##### 1. Initialization

- set the shift  $\sigma = \frac{1}{2}(\omega_{\min}^2 + \omega_{\max}^2)$
- select parameters:  $\xi, c_l, c_u, \varepsilon$
- set global cutoff values  $\lambda_{\min}^\sigma = -d_{\max}/\xi$  and  $\lambda_{\max}^\sigma = d_{\max}/\xi$
- set local cutoff values  $\mu_{\min}^\sigma = c_l \lambda_{\min}^\sigma$  and  $\mu_{\max}^\sigma = c_u \lambda_{\max}^\sigma$

##### 2. Compute $K_m^\sigma, M_m, b_m, l_m$ defined in (11)

##### 3. Compute the eigenpairs $(\Theta_n^\sigma, \Phi_n)$ of $(K_m^\sigma, M_m)$ specified by the global cutoff values $\lambda_{\min}^\sigma$ and $\lambda_{\max}^\sigma$

##### 4. Totaliter = 0

##### 5. FS loop for $k = 1, 2, \dots, n_f$

- calculate  $p_n(\omega_k)$  by (18)
- set the initial response  $p_t^0(\omega_k)$  by (30)
- niter( $k$ ) = 0

- (d) for  $\ell = 1, 2, \dots$
- (1) calculate residual  $r_m^{\ell-1}(\omega_k)$  by (22)
  - (2) calculate the correction  $\Delta p_t^\ell(\omega_k)$  by (28)
  - (3) test for convergence by (31)
  - (4) if stopping criterion is satisfied, then exit the  $\ell$ -loop
  - (5) compute  $p_t^\ell(\omega_k)$  by (29)
  - (6)  $\text{niter}(k) = \text{niter}(k) + 1$
  - (7) if  $\text{niter}(k) > \text{niter}_{\max}$ , convergence is failed, exit
- (e)  $p_m(\omega_k) = p_n(\omega_k) + p_t^\ell(\omega_k)$   
 (f)  $H_m(\omega_k) = L_m^T p_m(\omega_k)$   
 (g)  $\text{Totaliter} = \text{Totaliter} + \text{niter}(k)$

Note that for step 2, we use the AS method as outlined in Section 2. An implementation of the AS algorithm is available in the public domain package called ASEIG [8]. For step 3, we can use an implementation of SIL method available in ARPACK [13] with SuperLU [14] as a linear solver. Alternatively, one may use other implementations of the SIL method [2] with a sparse linear solver, such as MUMPS [15]. We should note that the CPU performance of the algorithm to be reported in Section 5 has not been optimized in the choice of eigensolvers of substructures.

A special case of the ASFRA is to use a zero shift  $\sigma = 0$  and retain all modes smaller than the cutoff value  $\lambda_{\max}^0$  as defined in (39). The resulting method is referred to as ASFRA<sup>0</sup>.

## 5. NUMERICAL EXPERIMENTS

In this section, we present two numerical examples to illustrate the performance of ASFRA and compare with the other methods for Hi-FRA. Two examples were developed in numerical simulation of MEMS resonators. Such a resonator is under an electrostatic actuation and utilized in various micro-devices such as angular rate sensors, bandpass filters and so on. An electrical signal is converted into the mechanical motion at the drive electrodes of the resonator. If the electrical input signal matches the mechanical natural frequency, the oscillation amplitude is increased, which is called a resonance. The oscillation converts into a current at the sense electrodes. A resonance behavior must be identified by an FRA in a product design process. The FRA of large-scale FE models in the high-frequency range is non-trivial and costly.

All experiments were conducted on an HP zx6000 workstation, which has 1.5 GHz Itanium II processors. This computer has 4 gigabytes (GB) of physical memory, and 80 GB of disk space. The operating system is RedHat Enterprise Linux AS Release 3.0.

### 5.1. Butterfly gyro

In this example, we employ a finite element (FE) model of a vibrating micro-mechanical gyro, called the Butterfly, for theoretical performance characterization in inertial navigation applications [16]. The FE model uses solid (3D) elements. The order of the stiffness and mass matrices  $K$  and  $M$  is  $N = 17631$ . Both matrices  $K$  and  $M$  are symmetric positive definite with the number of non-zero entries 519 260 and 178 896, respectively. The input and output vectors  $b$  and  $l$  have 8 and 1 non-zero elements, respectively.

The Rayleigh damping parameters  $\alpha$  and  $\beta$  are set as  $\alpha=0$  and  $\beta=1 \times 10^{-10}$ . Frequency responses go through rapid changes near the resonances in the range

$$[f_{\min}, f_{\max}] = [1.4, 1.5] \text{ MHz}$$

where we use the frequency  $f$  in Hz, instead of  $\omega$  in radian per second. Correspondingly,  $\omega_{\min} = 2\pi f_{\min}$  and  $\omega_{\max} = 2\pi f_{\max}$ . The frequency in Hz is easier to catch the physical meaning of the resonance rather than the frequency in radian, although mathematical expression using frequency in radian is simpler. We consider the calculation of the frequency responses  $H(2\pi f_k)$  at  $n_f = 201$  frequency point  $f_k$  in an equal space between  $f_{\min}$  and  $f_{\max}$ .

The required parameters of ASFRA, namely the shift  $\sigma$ , the number of substructuring levels  $l_v$ , contraction ratio  $\xi$  and relaxation factors  $c_l$  and  $c_u$  are set as the default values (see Section 4). Specifically, these parameters are

$$\sigma = \frac{1}{2}(\omega_{\min}^2 + \omega_{\max}^2) = \frac{(2\pi)^2}{2}(f_{\min}^2 + f_{\max}^2) = 8.31 \times 10^{13}$$

and

$$l_v = 3, \quad \xi = 0.5, \quad c_l = c_u = 10$$

Subsequently, the global cutoff values are

$$\lambda_{\min}^{\sigma} = -1.14 \times 10^{13} \quad \text{and} \quad \lambda_{\max}^{\sigma} = 1.14 \times 10^{13}$$

In other words, the retained eigenvalues of the original matrix pair  $(K, M)$  are in the interval

$$[\lambda_{\min}, \lambda_{\max}] = [\lambda_{\min}^{\sigma} + \sigma, \lambda_{\max}^{\sigma} + \sigma] = [7.17 \times 10^{13}, 9.45 \times 10^{13}]$$

The frequency responses  $H(2\pi f_k)$  computed by ASFRA, ASFRA<sup>0</sup>, SIL method and the direct method are shown Figure 1.

The direct method is to compute the frequency responses  $H(2\pi f_k)$  by first solving the linear system (2) using the SuperLU direct sparse solver [14].

The SIL method is an MS method. We first extract  $n$  eigenpairs of the original matrix pair  $(K, M)$  by SIL method from ARPACK [13]. Then we approximate  $H(\omega_k)$  by  $H_n(\omega_k)$  as defined in (4). The shift is  $\sigma=0$  and the eigenmodes are determined by an upper cutoff value  $\lambda_{\max} = (\chi\omega_{\max})^2$ , where  $\chi$  is a multiplication factor. Typically,  $\chi=2$  or  $3$ , when there are no residual flexibility vectors. Otherwise,  $\chi$  can be smaller, say  $\chi=1.11$  [17]. We note that if SIL uses  $\sigma$  from ASFRA, the residual flexibility vectors cannot be used. SIL needs to compute all eigenvalues below  $(2\omega_{\max})^2$  for obtaining similar accuracy.

The responses computed by ASFRA and SIL are visually indistinguishable from the response of the original system. We note that ASFRA has much better accuracy than ASFRA<sup>0</sup>. Figure 2 shows the relative errors for ASFRA and ASFRA<sup>0</sup>. The tolerance value for the stopping criterion (31) of the FS iteration (29) is  $\varepsilon = 10^{-5}$ .

The following table shows the dimension of the AS subspace, numbers of retained modes and the total FS iterations, and the elapsed time of computation.

	Direct	SIL	ASFRA <sup>0</sup>	ASFRA
<i>Butterfly gyro</i> , $N = 17631$				
$m$ (AS subspace)	—	—	651	213
$n$ (retained modes)	—	156	175	20
Total iter	—	—	51	238
Elapsed time (s)	754.6	80.42	62.94	26.77

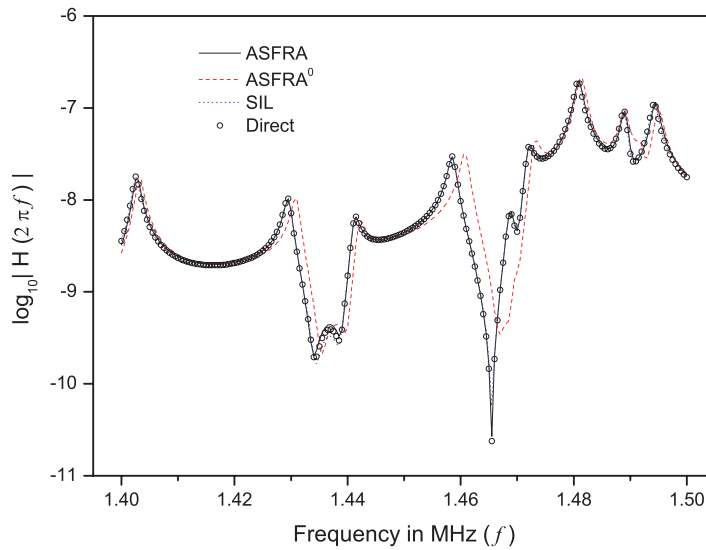


Figure 1. The frequency responses of Butterfly gyro computed by the direct method, SIL, ASFRA<sup>0</sup> and ASFRA.

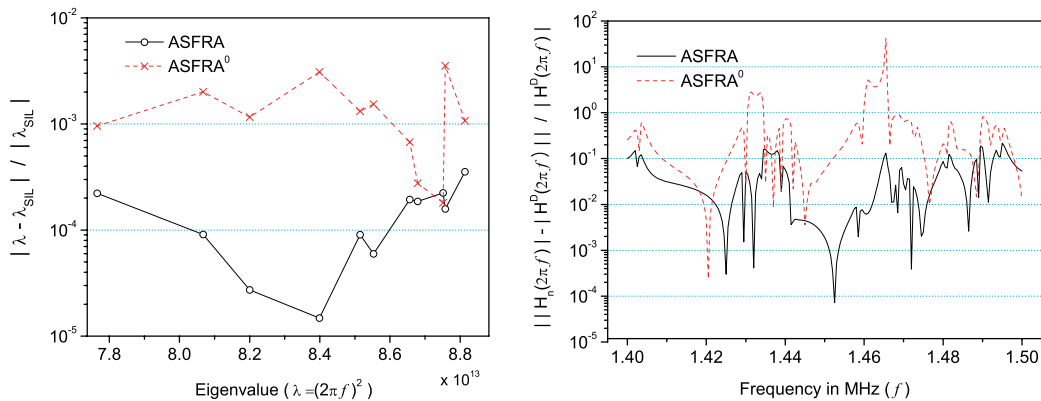


Figure 2. Left: The relative accuracy of the computed eigenvalues  $\lambda_k = (2\pi f_k)^2$  for  $f_k \in [f_{\min}, f_{\max}]$ . Right: The relative accuracy of frequency responses  $H(2\pi f_k)$  for  $f_k \in [f_{\min}, f_{\max}]$ .

From the table we see that ASFRA retains substantially less local and global modes to reach to the high-frequency range 1.4–1.5 MHz. It translates into substantial saving in the computational time. SIL is more expensive than ASFRA because it needs to obtain eigenmodes in full-size eigensystem of the original matrix pair  $(K, M)$ . In addition we note that often the initial guess  $p_i^0(\omega_k)$  by the linear extrapolation (30) may already be sufficiently accurate at some frequency points  $\omega_k$ . Therefore, no iterative refinement is required. Hence, the total number of FS iterations could be smaller than the number of frequency points to be calculated. This is true for the ASFRA<sup>0</sup> here.

The left plot of Figure 2 shows the relative errors of eigenvalues computed by ASFRA and ASFRA<sup>0</sup>, compared with the ones computed by the SIL. As one can see, the eigenvalues computed by ASFRA are more accurate than ASFRA<sup>0</sup>, in particular, when they are close to the shift  $\sigma$  near the middle of the interval. Although the number of retained modes is large, the accuracy of the ASFRA<sup>0</sup> is worse than ASFRA in the frequency range of interest, see right plot of Figure 2, where the relative error is defined as

$$\frac{||H_n(2\pi f_k)| - |H(2\pi f_k)||}{|H(2\pi f_k)|}$$

SIL is a global eigensolver. The accuracy of the eigenmodes computed by SIL is generally more accurate than the AS algorithm. We observe that the relative error of SIL is similar to the one of ASFRA.

### 5.2. Checkerboard filter

In this example, we present the performance of ASFRA on an FE simulation of a prototype checkerboard MEMS filter. The goal of this device is to produce a high-frequency bandpass filter, for example, the surface acoustic wave devices used in cell phones [18]. The order of stiffness and mass matrices  $K$  and  $M$  generated by the FE discretization of 2D elements is 15 258. Both  $K$  and  $M$  are symmetric positive definite with the number of non-zero elements 263 764 and 131 882, respectively. The input and output vectors  $b$  and  $l$  have 44 and 1 non-zero elements, respectively.

The Rayleigh damping parameters are set by  $\alpha = 1.0 \times 10^6$  and  $\beta = 0$ . Frequency responses changes rapidly near the resonances in the range

$$[f_{\min}, f_{\max}] = [210, 230] \text{ MHz}$$

We consider the calculation of the frequency responses  $H(2\pi f_k)$  at  $n_f = 201$  frequency point  $f_k$  in an equal space between  $f_{\min}$  and  $f_{\max}$ .

For ASFRA the shift  $\sigma$ , number of the substructuring levels  $l_v$ , contraction ratio  $\xi$  and relaxation factors  $c_l$  and  $c_u$  tolerance value  $\varepsilon$  are also set as the default values suggested in Section 4, i.e.

$$\sigma = \frac{1}{2}(\omega_{\min}^2 + \omega_{\max}^2) = \frac{(2\pi)^2}{2}(f_{\min}^2 + f_{\max}^2) = 1.91 \times 10^{18}$$

and

$$l_v = 3, \quad \xi = 0.5, \quad c_l = c_u = 10, \quad \varepsilon = 10^{-5}$$

Subsequently, the global cutoff values of the matrix pair  $(K_m^\sigma, M_m)$  are

$$\lambda_{\min}^\sigma = -3.47 \times 10^{17} \quad \text{and} \quad \lambda_{\max}^\sigma = 3.47 \times 10^{17}$$

In other words, the retained eigenvalues of the original matrix pair  $(K, M)$  are in the interval

$$[\lambda_{\min}, \lambda_{\max}] = [\lambda_{\min}^{\sigma} + \sigma, \lambda_{\max}^{\sigma} + \sigma] = [1.57 \times 10^{18}, 2.26 \times 10^{18}]$$

Figure 3 shows the frequency responses computed by ASFRA, ASFRA<sup>0</sup>, SIL and direct method. The responses computed by ASFRA<sup>0</sup> is visually worse than the responses, computed by the ASFRA, SIL and direct methods. The following table lists the dimension of the AS subspace, numbers of retained global modes and the FS iterations, and the computational elapsed time.

	Direct solution	SIL	ASFRA <sup>0</sup>	ASFRA
<i>Checkerboard filter, N = 15258</i>				
$m$ (AS subspace)	—	—	1424	278
$n$ (retained modes)	—	234	203	27
Total iter	—	—	98	660
Elapsed time (s)	1246.2	110.25	163.72	21.12

ASFRA retains substantial fewer local and global modes to reach to the high-frequency range 210–230 MHz. It translates into substantial saving in the computational elapsed time. ASFRA is about 7.7 times faster than the ASFRA<sup>0</sup>. SIL is about 5.2 times longer than ASFRA in computational time since it should obtain eigenmodes in full-size eigensystem with the original matrix pair  $(K, M)$ .

The left plot of Figure 4 shows the relative errors of eigenvalues computed by ASFRA and ASFRA<sup>0</sup>, compared with the ones computed by the SIL. As one can see, the eigenvalues computed by ASFRA are more accurate than ASFRA<sup>0</sup>, in particular, when they are close to the shift  $\sigma$  near

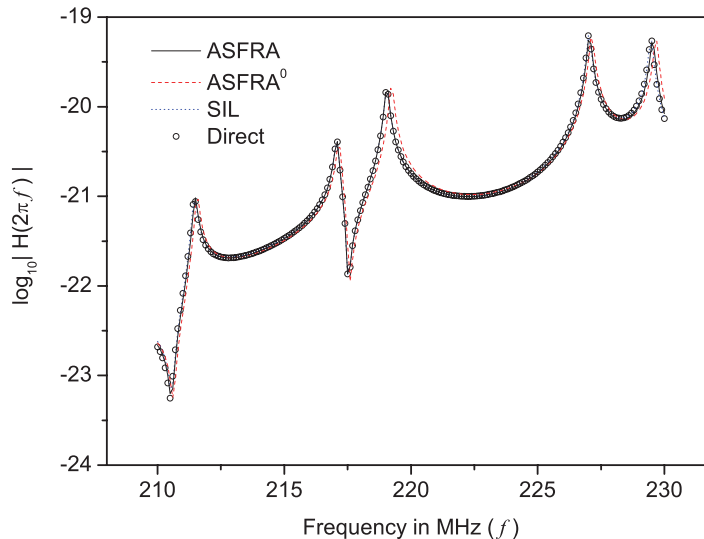


Figure 3. The frequency responses of checkerboard filter computed by the direct method, SIL, ASFRA<sup>0</sup> and ASFRA.

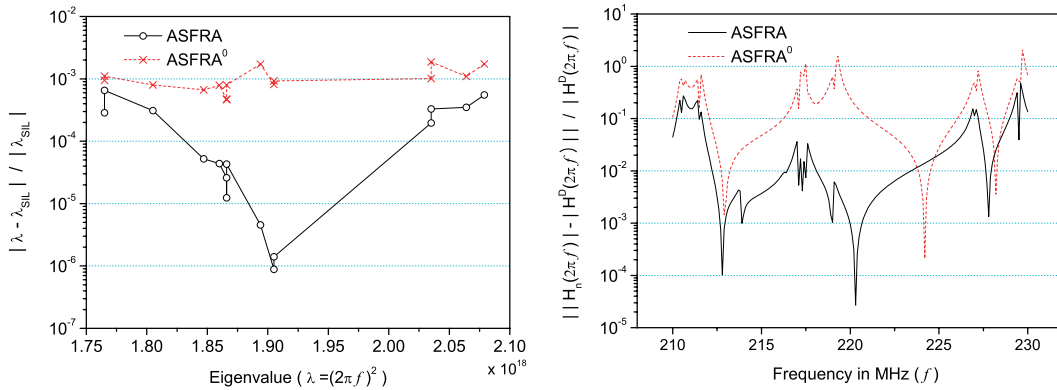


Figure 4. Left: The relative accuracy of eigenvalues  $\lambda_k = (2\pi f_k)^2$  for  $f_k \in [f_{\min}, f_{\max}]$ . Right: The relative accuracy of frequency responses  $H(2\pi f_k)$  for  $f_k \in [f_{\min}, f_{\max}]$ .

the middle of the interval. Subsequently, as shown in the right plot of Figure 4, ASFRA returns more accurate frequency responses in the frequency range of interest. For the record, the relative error of SIL is similar to the one of ASFRA.

### 5.3. The impact of parameters

We present a preliminary study on the impact of the choice of two key parameters, namely contraction ratio  $\xi$  and relaxation factor  $c_l$ , to the performance of ASFRA.

5.3.1. *Contraction ratio  $\xi$ .* The contraction ratio  $\xi$  determines the local and global cutoff values that control the number of retained modes and convergence rate of the FS iteration. For the Butterfly gyro case study, we investigate the effect of the CPU time under the variation of the contraction ratio  $\xi$ . The number of the local modes is kept at the constant  $m = 213$  by varying the relaxation factor  $c_l$ . This can be done since by the way of determining the local cutoff values  $\mu_{\min}^\sigma$  and  $\mu_{\max}^\sigma$ , once  $d_{\max}$  is fixed, one can vary  $c_l$  and  $\xi$  to keep the local cutoff values unchanged.

The following table shows the number of retained global modes ( $n$ ), total number of FS iterations (Totaliter), CPU time for computing the retained global modes and FS iteration and the total CPU of ASFRA.

$\xi$	$c_l$	$m$	$n$	Totaliter	$(\Theta_n^\sigma, \Phi_n)$ -CPU	FS-CPU	Total CPU
0.9	18	213	12	598	0.09	3.26	26.99
0.5	10	213	20	238	0.15	2.95	26.77
0.1	2	213	83	101	0.95	2.96	27.58

As the analysis of Section 3 indicates, a small  $\xi$  leads to a large number of retained modes  $n$  and, subsequently, leads to the fast convergence of the FS iteration. Note that the CPU time for FS iteration does not change significantly. Since the total CPU times does not considerably vary, the default value  $\xi = 0.5$  is a good choice for the comparison in Section 5.1. The following

table presents the similar data for the checkerboard filter case. It concurs with the findings of the Butterfly gyro.

$\xi$	$c_l$	$m$	$n$	Totaliter	$(\Theta_n^\sigma, \Phi_n)$ -CPU	FS-CPU	Total CPU
0.9	18	278	15	728	0.15	6.41	20.66
0.5	10	278	27	660	0.44	6.41	21.12
0.1	2	278	163	68	1.31	5.77	21.08

5.3.2. *The relaxation factor  $c_l$ .* The relaxation factor  $c_l$  ( $=c_u$ , by default) along with the global cutoff values  $\lambda_{\min}^\sigma$  and  $\lambda_{\max}^\sigma$  determines the number of local modes to be extracted. We explore how the relative errors and the CPU run time vary with respect to the change of the relaxation factor  $c_l$ . The following table shows how the number of local modes ( $m$ ) varies as relaxation factor  $c_l$  changes, and its effort on the maximum relative errors of the computed eigenvalues in  $[(2\pi f_{\min})^2, (2\pi f_{\max})^2]$  for the Butterfly gyro.

$c_l$	$\xi$	$m$	$\lambda_k$ maximum relative error	Total CPU
5	0.5	118	$1.69 \times 10^{-3}$	22.96
10	0.5	213	$3.54 \times 10^{-4}$	26.77
20	0.5	260	$1.65 \times 10^{-4}$	30.00

As we expect, as the relaxation factor  $c_l$  increases, the number of computed local modes increases. Subsequently, the relative error of the eigenvalues decreases and the CPU time increases. It can be observed from the table that the maximum relative error of the eigenvalues becomes less than 0.1% by the default value  $c_l=10$ . The following table presents similar data for the checkerboard filter. It concurs with our findings.

$c_l$	$\xi$	$m$	$\lambda_k$ maximum relative error	Total CPU
5	0.5	206	$1.75 \times 10^{-3}$	16.31
10	0.5	278	$6.53 \times 10^{-4}$	21.12
20	0.5	419	$2.51 \times 10^{-4}$	30.67

## 6. CONCLUDING REMARKS

In this paper we presented an algebraic-substructuring-based frequency response analysis (ASFRA) algorithm to calculate the frequency responses of a large-scale dynamical system of the form (1) between two specified frequencies  $\omega_{\min}$  and  $\omega_{\max}$ . ASFRA can be efficiently applied to Hi-FRA, as demonstrated by two examples of microelectromechanical sensors operated at 1–2 and 200–250 MHz ranges. To some extent, ASFRA generalizes the underlying algorithm and functionality of commercially viable AMLS technique. AMLS is designed for FRA up to a specific frequency  $\omega_{\max}$ , starting from the lowest. Future work includes the optimal choice of parameters and parallelization

techniques. The extension of ASFRA for the Hi-FRA of dynamical systems with non-proportional damping is also a subject of future study.

## ACKNOWLEDGEMENTS

J. H. K. was supported in part by Korea Research Foundation grant KRF-2005-214-D00015. J. H. K. and Z. B. were also supported in part by the NSF grant DMS-0611548. Most of this work was done while J. H. K. visiting the University of California, Davis. The authors wish to thank anonymous reviewers for their many helpful comments and suggestions.

## REFERENCES

1. Craig Jr RR. *Structural Dynamics: An Introduction to Computer Methods*. Wiley: New York, 1981.
2. Bai Z, Demmel J, Dongarra J, Ruhe A, van der Vorst H (eds). *Templates for the Solution of Algebraic Eigenvalue Problems: A Practical Guide*. SIAM: Philadelphia, PA, 2000.
3. Bennighof JK, Kim CK. An adaptive multi-level substructuring method for efficient modeling of complex structures. *Proceedings of the AIAA 33rd SDM Conference*, Dallas, TX, 1992; 1631–1639.
4. Bennighof JK, Kaplan MF. Frequency sweep analysis using multi-level substructuring, global modes and iteration. *Proceedings of 39th AIAA/ASME/ASCE/AHS Structures, Structural Dynamics and Materials Conference*, Long Beach, U.S.A., 1998.
5. Bennighof JK, Lehoucq RB. An automated multilevel substructuring method for eigenspace computation in linear elastodynamics. *SIAM Journal on Scientific Computing* 2004; **25**(6):2084–2106.
6. Kaplan MF. Implementation of automated multilevel substructuring for frequency response analysis of structures. *Ph.D. Thesis*, University of Texas at Austin, 2001.
7. Yang C, Gao W, Bai Z, Li X, Lee L, Husbands P, Ng E. An algebraic substructuring method for large-scale eigenvalue calculations. *SIAM Journal on Scientific Computing* 2005; **27**(3):873–892.
8. Gao W, Li XS, Yang C, Bai Z. An implementation and evaluation of the amls method for sparse eigenvalue problems. *Technical Report LBNL-57438*, Lawrence Berkeley National Laboratory, 2006.
9. Elssel K, Voss H. An *a priori* bound for automated multi-level substructuring. *SIAM Journal on Matrix Analysis and Applications* 2006; **28**:386–397.
10. Karypis G. *METIS*. Department of Computer Science and Engineering at the University of Minnesota, July 2006 (Available from: <http://www-users.cs.umn.edu/karypis/metis/metis/index.html>).
11. Craig Jr RR, Bampton MCC. Coupling of substructures for dynamic analysis. *AIAA Journal* 1968; **6**(7):1313–1319.
12. Saad Y. *Iterative Methods for Sparse Linear Systems*. SIAM: Philadelphia, PA, 2003.
13. Lehoucq R, Sorensen DC, Yang C. *Arpack User's Guide: Solution of Large-Scale Eigenvalue Problems with Implicitly Restarted Arnoldi Methods*. SIAM: Philadelphia, PA, 1998.
14. Demmel JW, Eisenstat SC, Gilbert JR, Li XS, Liu JWH. A supernodal approach to sparse partial pivoting. *SIAM Journal on Matrix Analysis and Applications* 1999; **20**(3):720–755.
15. Amestoy PR, Duff IS, L'Excellent J-Y. Multifrontal parallel distributed symmetric and unsymmetric solvers. *Computer Methods in Applied Mechanics and Engineering* 2000; **184**:501–520.
16. Lienemann J, Billger D, Rudnyi EB, Greiner A, Korvink JG. Mems compact modeling meets model order reduction: examples of the application of Arnoldi methods to microsystem devices. *The Technical Proceedings of the 2004 Nanotechnology Conference and Trade Show, Nanotech 04*, Boston, U.S.A., 2004.
17. Thomas B, Gu RJ. Structural-acoustic mode synthesis for vehicle interior using finite-boundary elements with residual flexibility. *International Journal of Vehicle Design* 2000; **23**:191–202.
18. Bindel D, Bai Z, Demmel J. *Model Reduction for RF MEMS Simulation*. Lecture Notes in Computer Science, vol. 3732. Springer: Berlin, 2006; 286–295.